Research Paper

Experimental Characterization of Sound Absorption for Composite Panel Made of Perforated Plate and Membrane Foam Layer

Van-Hai TRINH[(1)], Mu HE[(2)*]

[(1)] *Institute of Vehicle and Energy Engineering, Le Quy Don Technical University*
Hoang Quoc Viet, Hanoi, Vietnam

[(2)] *School of Mechanical Science and Engineering, Huazhong University of Science and Technology*
Wuhan, Hubei, China

[*]Corresponding Author e-mail: mu.he@foxmail.com

A recent key challenge in noise engineering is the development of structures or materials that achieve desirable acoustic performance in practical settings. Combinations of porous layers and perforated plates offer potential composite absorbers for various acoustic applications. The present work conducts experimental characterizations of sound absorption performance of absorbers based on membrane foams combined with perforated plates. Membrane foams with the well-controlled cell size and porosity are fabricated by milli-fluidic tools, whereas perforated plates are made within a tuned perforation ratio. The three-microphone method is used to perform the acoustic measurements. The results obtained from ten combination samples reveal that the sound absorption behavior of the foam-based layers can be successfully tailored and improved by a thin perforated plate within a reasonable hole diameter and spacing while maintaining the total thickness of the composite absorber.

Keywords: membrane foam; monodisperse; perforated plate; composite absorber; sound absorption.

1. Introduction

Undesirable or harmful outside sounds, produced primarily by mechanical equipment, daily activities, and industrial processes, have a significant impact on both human and equipment performance. Designing sound-absorbing materials for real-world applications is one of the most frequent issues faced by acoustic engineers (ATTENBOROUGH, VÉR, 2006). Along this path, man-made materials (e.g., cellular foams, fibrous structures, particle-packed media) are showing their great potential for various acoustic applications in civil, automotive and aerospace engineering (ARENAS, CROCKER, 2010). Due to the small size of the interconnected pores in porous media, the sound absorption performance of these materials is governed by the thermal and viscous dissipations occurring inside the pores (ALLARD, ATALLA, 2009). The relationship between the microstructure and the properties of porous

absorbers can be characterized by different approaches (SAGARTZAZU *et al.*, 2008), which can guide the design of the required sound absorption coefficients (SAC).

The most popular models for characterizing sound-absorbing materials fall into three main groups: semi-empirical, semi-phenomenological, and phenomenological ones (SAGARTZAZU *et al.*, 2008; ALLARD, ATALLA, 2009). With the help of analytical, numerical and experimental advances, our understanding of the material behavior is improving. A porous medium with a rigid skeleton is represented by two frequency-independent factors, namely the complex density and complex bulk modulus (known as the equivalent fluid method (ALLARD, ATALLA, 2009)). Based on this powerful framework, the functional properties of the acoustic materials can be well modeled and characterized. The effective macro-scale properties are then numerically determined by finite element analysis using three alternative methods (ZIELIŃSKI *et al.*, 2020):

direct numerical simulations, direct multiscale homogenization, and hybrid multiscale homogenization. In the first framework, acoustic properties can be estimated from the solution of the uncoupled (thermoviscous) linearised Navier–Stokes equations. In the second technique, the macro-scale complex characteristics are defined from dynamic viscous and thermal permeability functions computed directly by a multiscale model (see (Gasser *et al.*, 2005; Lee *et al.*, 2009)), while the third approach allows computing a set of transport properties (i.e., characteristic lengths, permeabilities, tortuosities) to derive the final acoustic absorption, (see (Park *et al.*, 2017; Trinh *et al.*, 2022b)). From these known macroscopic transports, the above complex factors can also be calculated by the semi-phenomenological models, such as the Johnson–Champoux–Allard–Pride–Lafarge (JCAPL) model, known as the 8-parameter model. Based on the standard tube testing, acoustical and non-acoustical parameters of sound absorbing materials can be determined directly or indirectly (Panneton, Olny, 2006; Olny, Panneton, 2008; Salissou, Panneton, 2010). With the help of advanced computing tools, the development of optimized properties of sound-absorbing materials can now be done through machine learning and artificial intelligence approaches, where the computational cost can be significantly reduced by generating new data from the limited computational or experimental data (Zhang *et al.*, 2021; Trinh *et al.*, 2022a).

Owning to the high sound absorption, foam-based absorbers have been widely developed based on the theoretical understanding, simulation knowledge or experimental evidence (Yang *et al.*, 2015; Park *et al.*, 2017; Langlois *et al.*, 2020). For single foam layers at different pore scales (Trinh *et al.*, 2019; Langlois *et al.*, 2020), various local morphologies ranging from open-cell (Langlois *et al.*, 2020; Trinh *et al.*, 2022b) to membrane (Trinh *et al.*, 2019) structures have been designed by either the typical foaming process (Park *et al.*, 2017; Trinh *et al.*, 2019) or the 3D-printing technique (Zieliński *et al.*, 2022). On the other hand, several references have demonstrated a great improvement (e.g., low-frequency or high average absorption) in the absorption capacity by using multi-layer (Boulvert *et al.*, 2019) or composite (Trinh *et al.*, 2022b; Borelli, Schenone, 2021) absorbers filled with foams or fibers, and perforated plates can be employed as the potential sub-layers in composite absorbers for tuning the overall system response (Liu *et al.*, 2017; Duan *et al.*, 2019).

The noise control engineering often requires specific acoustic properties for a wide frequency range (Boulvert *et al.*, 2019) and other functions, e.g., anti-flaming, high strength, and high heat conduction (Gasser *et al.*, 2005; Jafari *et al.*, 2020; Kosała, 2024). For this reason, a systematic investigation of

the sound absorption of composite absorbers based on solid foam and perforated plate should be addressed. In this respect, the inner components of the composite absorbers (CA) considered in this study are membrane foams with controlled cell size and some configurations of perforated facings, and the absorption peaks as the quarter-wavelength resonances of the foam layer are modified by the presence of perforated facing.

2. Materials and experiments

Figure 1 illustrates the structure of the composite absorber, which includes a membrane foam layer and a facing perforated plate.
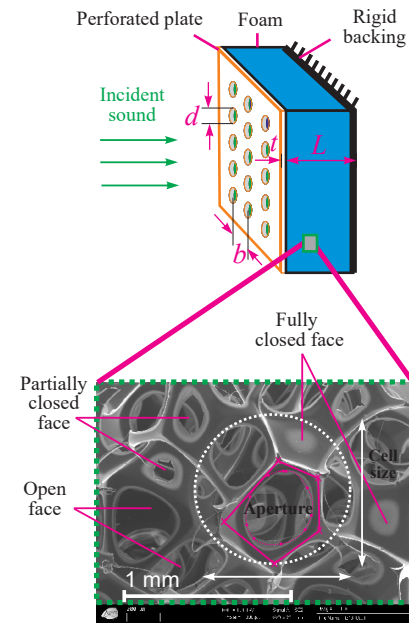

Fig. 1. Illustration of the sound absorber configuration and the foam characteristics.

Table 1. Geometrical parameters of the perforated plates.

Plate	Hole diameter d [mm]	Hole spacing b [mm]	Perforation ratio p [–]
PP1	0.5	4.0	0.012
PP2	1.0	4.0	0.049
PP3	0.5	2.0	0.049
PP4	1.5	4.0	0.110
PP5	1.0	2.0	0.196

The monodisperse foam material is fabricated as follows (Trinh *et al.*, 2019):

1) a precursor aqueous foam and a gelatin solution are prepared: the precursor foam within a controlled bubble size ~810 (±30) μm and a constant liquid fraction of 0.99 is generated in a glass column by tuning the flow rates of nitrogen and foaming liquid (i.e., Tetradecyltrimethylammonium bromide (TTAB) at 3 g/L). On the other

hand, the aqueous gelatin solution, within a tuned mass concentration from 12 % to 18 %, is prepared and maintained at $T \sim 60\,°C$ (above the sol–gel transition temperature $\sim 30\,°C$);

2) then, the precursor foam is mixed with the hot gelatin solution, and their flow rates are adjusted to get the gas fraction of 0.8. The foaming mixture is filled into a 40 mm-diameter cylindrical cell with a length of 40 mm. To avoid gravity effects during the decreasing temperature process, the material cell is rotated (~ 50 rpm) around its axis;

3) the cell is stored in a climatic chamber for one hour at $5\,°C$ then one week at $T = 20\,°C$ and RH = 30 % for water evaporating. Finally, after unmolding, a 20 mm-thick specimen for acoustic tests is cut from the central region along the cell axis.

The density and the air flow resistance of the membrane foam samples are defined as follows. For the density, with the specific gravity of the dried gelatin measured to be $g_g = 1.36$, the density of the cut foam sample (diameter – $D = 40$ mm, and thickness – $L = 20$ mm) was calculated from the the sample mass m_s as $\rho_s = 10^{-6} m_s/V_s$ with $V_s = \frac{\pi D^2}{4} L$. This gives the density and the open porosity of the foam samples as $\rho_s = 27.1\ (\pm 2.3)$ kg/m^3 and $\phi = 0.98\ (\pm 0.003)$. The air flow resistance can be estimated from the air flow resistivity σ of the sample through the formula $R_s = \sigma L$. For the foam with low air flow resistivity, we have $\sigma = A\Delta P/Q$, where A is the sample cross-section area and ΔP is the measured pressure drop, and Q is the air flow rate. For the sample with high air flow resistivity, the value of σ can be inversely characterized as $\sigma = \lim_{\omega \to 0}[\Im(\omega \rho_{eq})]$, where ρ_{eq} is the effective density measured from the impedance tube test (see (PANNETON, OLNY, 2006)). Among the two test foam samples, only sample $F1$ allows for direct measurement of resistivity $\sigma = 10700$ Nsm^{-4} which is very similar to the characterized value shown in Table 2.

The cell size of the final foam layers measured from SEM images is 810 µm within the monodisperse structure. The membranes range from open to closed cells depending on the gelatin concentration used. Two specimens are selected, namely $F1$ and $F2$, within a moderate membrane fraction. As illustrated in the bottom part of Fig. 1, morphological characterizations can be undertaken to measure the membrane fractions of fully open or fully closed faces and the ratio of closure membrane (i.e., aperture/face area) in partially open ones, a detailed description of the

foam characterization can be found in (TRINH *et al.*, 2019).

Five stainless steel perforated plates (PP) with different configurations are manufactured. The geometrical parameters of the PP (Fig. 1, see the top part) are detailed in Table 1. For a square array, the perforation ratio is given as $p = \pi d^2/(4b^2)$. These plates have a thickness of $t = 1$ mm and a diameter of 40 mm. It should be noted that this diameter matches the size of the cut cylindrical foam samples to fit the inner diameter of the impedance tube for acoustic experiments.
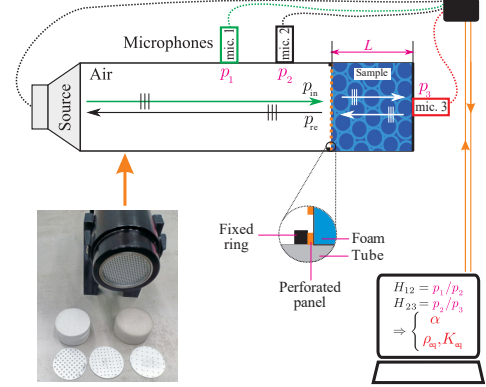

Fig. 2. Experimental setup of three-microphone impedance tube (length – 1 m, diameter – 40 mm).

Acoustic properties are measured using a three-microphone impedance tube (SALISSOU, PANNETON, 2010) in the frequency range of $f \in [4, 4500]$ Hz with a step of 4 Hz; see Fig. 2. Note that the perforated plate is placed adjacent to the foam layer without any bonding layers or membranes. Here, a steel ring (with an internal diameter of 39 mm and a square wire size of 1 mm) is used to hold the two material layers in the horizontal test tube. The SAC at normal incidence α is measured through the pressure transfer function H_{12} between microphones 1 and 2. Another function H_{23} between microphones 2 and 3 is used for direct evaluations of the equivalent properties (i.e., density ρ_{eq} and bulk modulus K_{eq}) and inverse estimations of the macroscopic transports (i.e., thermal characteristic length Λ', viscous characteristic length Λ, static air flow resistivity σ, thermal permeability k_0', and tortuosity α_∞ (PANNETON, OLNY, 2006; OLNY, PANNETON, 2008)). Based on the data obtained from the impedance tube experiment, the characterized transport properties of the two foam samples are estimated, see Table 2. In the next section, the results of the absorption properties of the foam layers and the composite absorbers are evaluated.

Table 2. Characterized macroscopic transport parameters of the foam samples.

Sample	Λ' [µm]	Λ [µm]	σ [Nsm^{-4}]	k_0' [$\times 10^{-10}$ m^2]	α_∞ [–]
$F1$	220 (± 36)	73 (± 14)	11560 (± 750)	109 (± 25)	2.48 (± 0.26)
$F2$	180 (± 30)	55 (± 8)	17500 (± 1200)	93 (± 19)	4.05 (± 0.33)

3. Results and discussion

The SAC curves of the single-layer foams and the perforated plates backed by an air gap of 7 mm are provided in Fig. 3. In terms of the acoustic properties of porous materials with membrane structures, a comparison between the measured data (solid line) the characterized absorption values (dashed line with circle markers) shows a high degree of agreement, as depicted in Fig. 3a. Note that computed sound absorption curves are defined from the semi-phenomenological model (i.e., Johnson–Champoux–Allard–Lafarge model). The results of the transport properties demonstrate consistency with previously obtained results for monodisperse foams with a thin solid membrane (TRINH et al., 2019) as well as foam materials with a high polydispersity of the pore size (NGUYEN et al., 2024). Both foam layers show a quarter-wavelength resonance behavior with $\alpha \sim 1$ at the central frequency of the first peak, $\widehat{f_1}$ (Fig. 3a). The results $\widehat{f_1}$ = 2132 Hz (Δf = 1888 Hz) and $\widehat{f_1}$ = 1392 Hz (Δf = 884 Hz) are, respectively, for $F1$ and $F2$, where Δf is the peak width at α = 0.8. It is clear that the high membrane foam $F2$ provides broadband performance (i.e., an absorption peak at lower frequencies) compared with the foam $F1$. However, when the membrane ratio in the foam sample is too high, causing the cell faces to be nearly closed, the absorption capability of the foam layer decreases because airborne waves cannot easily propagate into the foam structure (TRINH et al., 2019). The foam thickness of 20 mm is much smaller than the optimal thickness of granular-packed layers (>100 mm) to

achieve the above peaks, see Eq. (42) in (VIET DUNG et al., 2019). As depicted in Fig. 3b, the effect of perforation ratios on the sound absorption indicates that reducing the ratio p leads to an increase in the absorption, which is consistent with the findings in (LIU et al., 2017), while the plates PP2 and PP3 have the same perforation rate, they have different airflow resistivity (i.e., viscous permeability) and viscous characteristic lengths (due to different hole diameters) and these properties are responsible for different sound absorption performances. It should be noted that to clearly illustrate the absorption characteristics of perforated plates within different perforation ratios in the test frequency range, an air gap of 7 mm was chosen as an example within the range of 2 mm to 8 mm, as used in (LIU et al., 2017).

As shown in Fig. 4, thin perforated plates change significantly the acoustic behavior of the base foams. Herein, the configuration CAij denotes the combination of the foam Fi with the perforated plate PPj with $i = \{1, 2\}$ and $j = \{1, ..., 5\}$. The original absorption curves are generally shifted towards lower frequencies by combining PPs within a low ratio p, and the shift distance depends on the original peak or complex wavelength $\lambda_e = \sqrt{K_{eq}/\rho_{eq}}\big/f$. In detail, the frequency $\widehat{f_1}$ of the foam $F1$ is significantly reduced to 1316 Hz (e.g., CA11 in Fig. 4a), whereas it can be challenging to reduce that of the high-membrane foam $F2$ (i.e., $\widehat{f_1}$ = 1252 Hz for CA23, Fig. 4b). In contrast, the use of PPs with a high perforation ratio can improve the absorption capacity of the composite panels
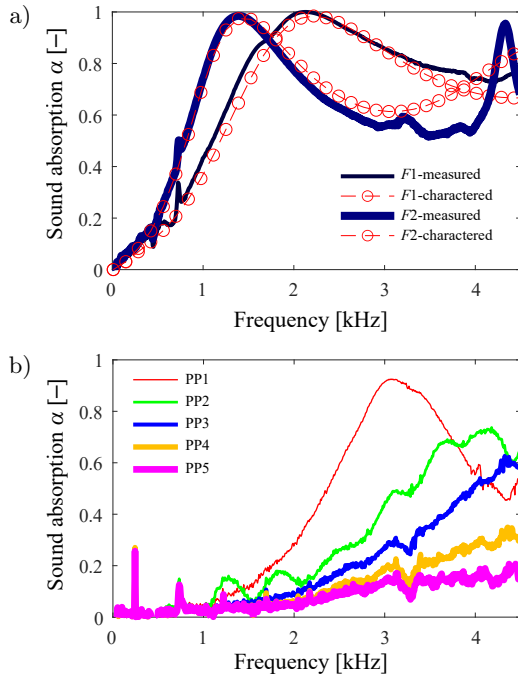

Fig. 3. Normal incidence sound absorption coefficients of (a) foam layers and (b) perforated plates backed by an air gap of 7 mm.
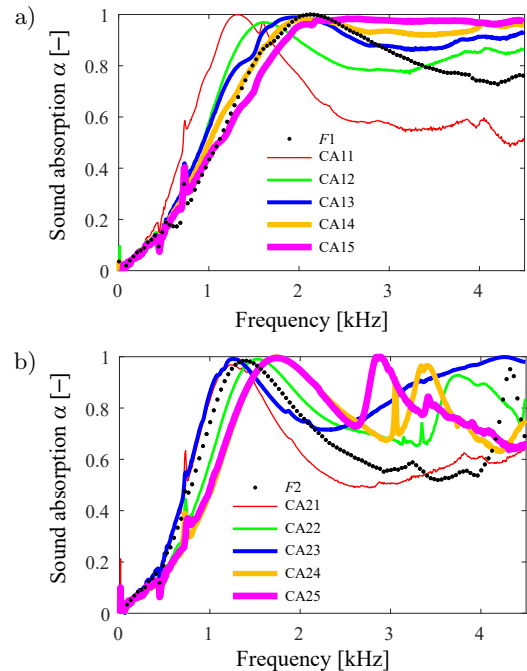

Fig. 4. Normal incidence sound absorption coefficients of composite absorbers based on foam $F1$ (a) and foam $F2$ (b).

in the high frequency range (see CAi3 to CAi5 for both foams). These observations confirm the link between the absorption property of CA and the imposed PP structure described in (DUAN *et al.*, 2019). Furthermore, the stably high absorption of CA14 and CA15 (Fig. 4a) behaves like a thick fibrous layer (SOLTANI, NOROUZI, 2020). In terms of modeling the structure studied (i.e., the perforated plate combined with an air layer or a foam layer), the assumption of rigid-frame porous models can be used with the necessary tortuosity correction (ATALLA, SGARD, 2007).

In order to rate the sound absorption performance of the test absorbers, the sound absorption coefficients on a set of ¹/₃ octaves from 200 Hz to 2500 Hz are used for evaluation. According to the (ASTM C423-23, 2023), two rating index numbers (i.e., the sound absorption average (SAA) and the noise reduction coefficient (NRC)) are calculated. Noted that the SAA and NRC are, respectively, calculated over the twelve ¹/₃ octave bands (from 200 Hz to 2500 Hz) and four frequencies (i.e., 250 Hz, 500 Hz, 1000 Hz, and 2000 Hz), and two rating results are approximately estimated from the field induced by normal incidence. As shown in Table 3, most of the composite absorbers based on foam $F1$ show a clear improvement in the rating index number (i.e., SAA = 0.49 and NRC = 0.50), while only the configuration CA23 shows the same behavior due to the peak occurring at the frequency of 1275 Hz. It can be said that by using a foam layer with a low membrane ratio (i.e., foam $F1$), we can easily shift the peak of the absorption curve to a lower frequency band.

Table 3. Rating of sound absorption of the test samples.

Test absorbers	Rating index	
	SAA [–]	NRC [–]
$F1$	0.41	0.45
CA11	0.49	0.50
CA12	0.44	0.45
CA13	0.45	0.45
CA14	0.43	0.45
CA15	0.41	0.45
$F2$	0.47	0.50
CA21	0.45	0.45
CA22	0.44	0.45
CA23	0.49	0.50
CA24	0.42	0.45
CA25	0.42	0.45

The absorption coefficients are next averaged as $\overline{\alpha} = (1/N) \sum_{i=1}^{N} \alpha(f_i)$ over N discrete frequencies f_i in [200, 1500] Hz for the low range and [1500, 4000] Hz for the high range (BOULVERT *et al.*, 2019; TRINH *et al.*, 2021). With a test frequency step of 4 Hz, N takes the values of 325 and 625, corresponding to the low-frequency range and high-frequency range, re-

spectively. By lowering the value of $\widehat{f}_1$, the average sound absorption of CA11 to CA14 (Fig. 5a) shows an improvement in the low frequency range. The absorption $\overline{\alpha}$ of CA11 increases approximately 1.5 times to reach ~0.6 (see the highest bar in low group in Fig. 5a), which could be the limit for all composite panels based on the foam $F2$ (low group in Fig. 5b). In high groups, the values $\overline{\alpha}$ averaging from configurations CAi3 to CAi5 are 0.934 for $i = 1$ (foam $F1$) and 0.840 for $i = 2$ (foam $F2$); the ratios between the value $\overline{\alpha}$ of the two-layer composite panels and that of the foam layer are calculated as 1.06 and 1.29, respectively. These observations provide quantitative evidence of the absorption performance of composite panels. Based on PP3 with a medium perforation ratio and small holes, both CAi3 configurations exhibit improved sound absorption over the whole frequency range of interest.
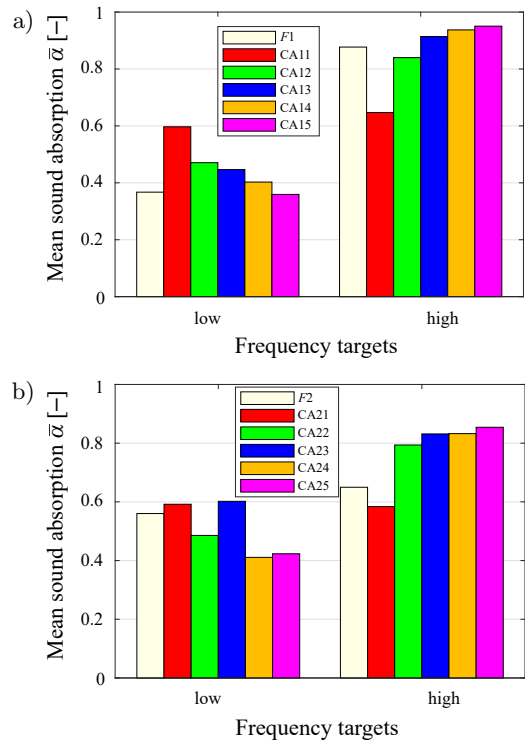
Fig. 5. Bar graphs of the average sound absorption of (a) foam $F1$ + plates PPj and (b) foam $F2$ + plates PPj.

4. Conclusions

In this paper, the sound absorption of foam layers covered by perforated plates has been experimentally characterized. The experimental evidence reveals the effects of the membrane level and the perforation parameters on the local absorption resonances (i.e., modified quarter-wavelength resonances of the foam layer within the influence of the facing perforated plate). The absorption behavior of a given foam material can be effectively tailored to the desired performance by adding appropriate perforated facings. Perforated

plates with a low perforation ratio are advantageous for low-frequency sound absorption applications and vice versa. In addition, good sound absorption over the full frequency range can be achieved by using composite layers with a fixed thickness of about ~20 mm. Based on the present framework, further works can be designed for the systematic characterization of composite absorbers developed for real applications.

Acknowledgments

References

1. ALLARD J.F., ATALLA N. (2009), *Propagation of Sound in Porous Media: Modelling Sound Absorbing Materials*, 2nd ed., JohnWiley & Sons.

2. ARENAS J.P., CROCKER M.J. (2010), Recent trends in porous sound-absorbing materials, *Sound & Vibration*, **44**(7): 12–18.

3. ASTM C423-23 (2023), *Standard test method for sound absorption and sound absorption coefficients by the reverberation room method*, ATM International, https://doi.org/10.1520/C0423-22.

4. ATALLA N., SGARD F. (2007), Modeling of perforated plates and screens using rigid frame porous models, *Journal of Sound and Vibration*, **303**(1–2): 195–208, https://doi.org/10.1016/j.jsv.2007.01.012.

5. ATTENBOROUGH K., VÉR I.L. (2006), Sound-absorbing materials and sound absorbers, [in:] *Noise and Vibration Control Engineering: Principles and Applications*, VÉR I.L., VERANEK L.L. [Eds.], 2nd ed., John Wiley & Sons, https://doi.org/10.1002/9780470172568.ch8.

6. BORELLI D., SCHENONE C. (2021), On the acoustic transparency of perforated metal plates facing a porous fibrous material, *Noise Mapping*, **8**(1): 185–203, https://doi.org/10.1515/noise-2021-0014.

7. BOULVERT J. *et al.* (2019), Optimally graded porous material for broadband perfect absorption of sound, *Journal of Applied Physics*, **126**(17): 175101, https://doi.org/10.1063/1.5119715.

8. DUAN H., SHEN X., YANG F., BAI P., LOU X., LI Z. (2019), Parameter optimization for composite structures of microperforated panel and porous metal for optimal sound absorption performance, *Applied Sciences*, **9**(22): 4798, https://doi.org/10.3390/app9224798.

9. GASSER S., PAUN F., BRÉCHET Y. (2005), Absorptive properties of rigid porous media: Application to face centered cubic sphere packing, *The Journal of the Acoustical Society of America*, **117**(4): 2090–2099, https://doi.org/10.1121/1.1863052.

10. JAFARI M.J., KHAVANIN A., EBADZADEH T., FAZLALI M., SHARAK M.N., MADVARI R.F. (2020), Optimization of the morphological parameters of a metal foam for the highest sound absorption coefficient using local search algorithm, *Archives of Acoustics*, **45**(3): 487–497, https://doi.org/10.24425/aoa.2020.134066.

11. KOSAŁA K. (2024), Modelling the acoustic properties of baffles made of porous and fibrous materials, *Archives of Acoustics*, **49**(3): 345–357, https://doi.org/10.24425/aoa.2024.148792.

12. LANGLOIS V., KADDAMI A., PITOIS O., PERROT C. (2020), Acoustics of monodisperse open-cell foam: An experimental and numerical parametric study, *The Journal of the Acoustical Society of America*, **148**(3): 1767–1778, https://doi.org/10.1121/10.0001995.

13. LEE C.-Y., LEAMY M.J., NADLER J.H. (2009), Acoustic absorption calculation in irreducible porous media: A unified computational approach, *The Journal of the Acoustical Society of America*, **126**(4): 1862–1870, https://doi.org/10.1121/1.3205399.

14. LIU Z., ZHAN J., FARD M., DAVY J.L. (2017), Acoustic properties of multilayer sound absorbers with a 3D printed micro-perforated panel, *Applied Acoustics*, **121**: 25–32, https://doi.org/10.1016/j.apacoust.2017.01.032.

15. NGUYEN C.T., LANGLOIS V., GUILLEMINOT J., DUVAL A., PERROT C. (2024), Effect of pore size polydispersity on the acoustic properties of high-porosity solid foams, *Physics of Fluids*, **36**(4): 047101, https://doi.org/10.1063/5.0191517.

16. OLNY X., PANNETON R. (2008), Acoustical determination of the parameters governing thermal dissipation in porous media, *The Journal of the Acoustical Society of America*, **123**(2): 814–824, https://doi.org/10.1121/1.2828066.

17. PANNETON R., OLNY X. (2006), Acoustical determination of the parameters governing viscous dissipation in porous media, *The Journal of the Acoustical Society of America*, **119**(4): 2027–2040, https://doi.org/10.1121/1.2169923.

18. PARK J.H. *et al.* (2017), Optimization of low frequency sound absorption by cell size control and multiscale poroacoustics modeling, *Journal of Sound and Vibration*, **397**(9): 17–30, https://doi.org/10.1016/j.jsv.2017.03.004.

19. SAGARTZAZU X., HERVELLA-NIETO L., PAGALDAY J.M. (2008), Review in sound absorbing materials, *Archives of Computational Methods in Engineering*, **15**(3): 311–342, https://doi.org/10.1007/s11831-008-9022-1.

20. SALISSOU Y., PANNETON R. (2010), Wideband characterization of the complex wave number and characteristic impedance of sound absorbers, *The Journal of the Acoustical Society of America*, **128**(5): 2868–2876, https://doi.org/10.1121/1.3488307.

21. SOLTANI P., NOROUZI M. (2020), Prediction of the sound absorption behavior of nonwoven fabrics: Computational study and experimental validation, *Journal of Sound and Vibration*, **485**: 115607, https://doi.org/10.1016/j.jsv.2020.115607.

22. TRINH V.H., GUILLEMINOT J., PERROT C. (2021), On the sensitivity of the design of composite sound absorbing structures, *Materials & Design*, **210**: 110058, https://doi.org/10.1016/j.matdes.2021.110058.

23. TRINH V.H., GUILLEMINOT J., PERROT C., VU V.D. (2022a), Learning acoustic responses from experiments: A multiscale-informed transfer learning approach, *The Journal of the Acoustical Society of America*, **151**(4): 2587–2601, https://doi.org/10.1121/10.0010187.

24. TRINH V.H., LANGLOIS V., GUILLEMINOT J., PERROT C., KHIDAS Y., PITOIS O. (2019), Tuning membrane content of sound absorbing cellular foams: Fabrication, experimental evidence and multiscale numerical simulations, *Materials & Design*, **162**: 345–361, https://doi.org/10.1016/j.matdes.2018.11.023.

25. TRINH V.-H., NGUYEN T.-V., NGUYEN T.-H.-N., NGUYEN M.-T. (2022b), Design of sound absorbers based on open-cell foams via microstructure-based modeling, *Archives of Acoustics*, **47**(4): 501–512, https://doi.org/10.24425/aoa.2022.142894.

26. VIET DUNG V., PANNETON R., GAGNÉ R. (2019), Prediction of effective properties and sound absorption of random close packings of monodisperse spherical particles: Multiscale approach, *The Journal of the Acoustical Society of America*, **145**(6): 3606–3624, https://doi.org/10.1121/1.5111753.

27. YANG X., REN S., WANG W., LIU X., XIN F., LU T. (2015), A simplistic unit cell model for sound absorption of cellular foams with fully/semi-open cells, *Composites Science and Technology*, **118**: 276–283, https://doi.org/10.1016/j.compscitech.2015.09.009.

28. ZHANG H., WANG Y., LU K., ZHAO H., YU D., WEN J. (2021), SAP-Net: Deep learning to predict sound absorption performance of metaporous materials, *Materials & Design*, **212**: 110156, https://doi.org/10.1016/j.matdes.2021.110156.

29. ZIELIŃSKI T.G. *et al.* (2022), Taking advantage of a 3D printing imperfection in the development of sound-absorbing materials, *Applied Acoustics*, **197**: 108941, https://doi.org/10.1016/j.apacoust.2022.108941.

30. ZIELIŃSKI T.G., VENEGAS R., PERROT C., ČERVENKA M., CHEVILLOTTE F., ATTENBOROUGH K. (2020), Benchmarks for microstructure-based modelling of sound absorbing rigid-frame porous media, *Journal of Sound and Vibration*, **483**: 115441, https://doi.org/10.1016/j.jsv.2020.115441.